

Senior Research

Specular Reflectance of Substrates Used in Printing

Final Report

Jeffrey P. Wible
Chester F. Carlson Center for Imaging Science
Rochester Institute of Technology
May 2005

Copyright © 2005
Center for Imaging Science
Rochester Institute of Technology
Rochester, NY 14623-5604

This work is copyrighted and may not be reproduced in whole or in part without permission of the Center for Imaging Science at the Rochester Institute of Technology.

This report is accepted in partial fulfillment of the course 1051-503 Senior Research.

Title: Specular Reflectance of Substrates Used in Printing
Author: Jeffrey P. Wible
Project Advisor: Jonathan Arney, Ph.D.
1051-503 Instructor: Joseph P. Hornak

Specular Reflectance of Substrates Used in Printing

Jeffrey P. Wible

Center for Imaging Science
Rochester Institute of Technology
Rochester, NY 14623-5604

May 16, 2005

Abstract

Specular gloss is an important factor in the development and utilization of printable substrates. A common method of measuring specular gloss is to use a standard gloss meter, several of which have been developed over the years by various research firms. However, gloss meters provide only a single number index of specular reflectance. A micro-goniophotometer has recently been developed in this laboratory for measuring the entire goniophotometric curve (BRDF) of specular light reflected from substrate samples. This provides significantly more information about gloss than is available from simple gloss meters.

The micro-goniophotometer was used in this project to explore the mechanism of specular reflection from a variety of coated and non-coated papers. The results of the study indicated that some coated sheets reflect specular light not only from the first surface of the coating but also from the sub-surface boundary between the coating and the paper. Analysis of the shapes of the BRDF curves was also carried out. The height/width ratio was found to be the major correlate with traditional gloss, and the total specular reflection factor was not found to contribute significantly to differences in substrate gloss as measured by traditional meters.

The results of this project have demonstrated the utility of micro-goniophotometric analysis. It is a relatively simple instrument capable of providing significantly more information about gloss than is available by other means.

Acknowledgements

I would like to extend my sincerest thanks to Dr. Jon Arney for his advice on this project, Sue Chan for her outstanding academic and moral support over the years, Alvin Spivey for a wealth of motivation and friendship, and my parents, Joy and Douglas Wible, for their irreplaceable love and support which will always be my guide.

Table of Contents

Copyright Release	i
Abstract	ii
Acknowledgements	iii
Table of Contents	iv
1 Introduction	1
2 Background	2
3 Experimental Methods	5
3.1 Instrument Design	5
3.2 Data Collection	6
4 Procedure	9
4.1a BRDF Area Analysis	10
4.1b Results and Discussion	11
4.2a BRDF Shape Analysis	12
4.2b Results and Discussion	14
4.3a BRDF and Standard Gloss	15
4.3b Results and Discussion	16
5 Final Discussion and Conclusions	17
6 References	20
7 Appendix	21
7.1 Index of Substrate Samples	21

1 Introduction

Anecdotal experience suggests that there are several properties of gloss that play a role in the perception of a printed image. Specular light certainly plays a crucial role in the visual effects of gloss. However, the specular reflections from complex, rough surfaces are not well understood, and traditional techniques for measuring specular light have not provided sufficient insight into these optical mechanisms. The work described in this report was undertaken in order to explore the mechanism of specular reflection from a variety of paper types commonly used in printing processes. The experimental work in this project was done with a micro-goniophotometer recently developed in this laboratory¹. As will be shown, this instrument was able to provide significant insights into the nature of specular reflections from printing substrates.

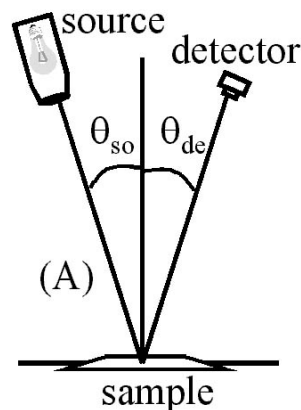
2 Background

The concept of “gloss” is intuitively easy to understand. It is the bright glint that results from holding glossy objects at a particular angle relative to a light source. This gloss angle is the equal/opposite angle characteristic of a mirror reflection, and so gloss light is often called specular light, from the Latin for mirror; or Fresnelian light, after the person who described the optical laws of specular reflection.

The Fresnelian light reflected from a printed surface is typically not the light one wishes to observe, and so one holds the print at an angle that eliminates the gloss. The light one does want to see is the light reflected by a different optical mechanism. This other reflection mechanism involves the penetration of light into the bulk of the ink and paper, scattering in the system, and reflection in all angular directions from -90° to $+90^\circ$. This light carries the color and shape information of the printed image and is called bulk reflected light, or Lambertian light after the person who described the optical laws of bulk scattered reflection. So, the light reflected from a surface can be categorized into two types; Lambertian reflection and specular reflection. Lambertian reflection refers to light that penetrates to a certain depth in the surface, where a combination of scattering and absorption occur. Lambertian light is reflected in all angular directions from -90° to $+90^\circ$.

Qualitatively, specular reflections and Lambertian reflections are easily distinguished. Lambertian light is reflected at all angles, but specular light is reflected only at the specular angle, θ , which is the angle equal to but opposite from the angle of incidence. For this reason, gloss is typically measured with a gloss meter designed to illuminate a surface with collimated light from a specified angle θ_{so} and measure irradiance from the equal and opposite detection angle θ_{de} , as illustrated in Figure 1^{4,6}.

Figure 1: Basic design of a gloss meter; sample is illuminated at illumination angle, θ_{so} , and reflected light is measure at equal and opposite angle, θ_{de} .¹



Many commercially available gloss meters allow measurements to be made at angles ranging from 20° to 75° ³. In accordance with Fresnel's laws, gloss increases as the gloss angle increases. For this reason, high gloss materials are measured at low angles (e.g. 20°) and low gloss materials such as plain paper are generally measured at high angles (e.g. 75°)³.

If the surface in question was a perfectly reflective mirror, then the instrument outlined in Figure 1 would be more than sufficient at characterizing gloss. However, paper and other printable substrates are not perfectly smooth but rather have minute variations in surface topography. Specular light is therefore reflected over a range of angles around the mean specular angle, θ , as illustrated in Figures 2 and 3.

Figure 2: Illustration of collimating lenses in a standard gloss meter³

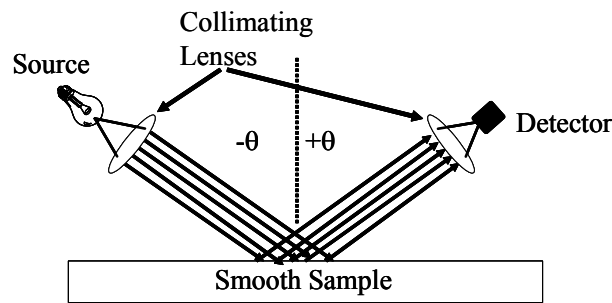
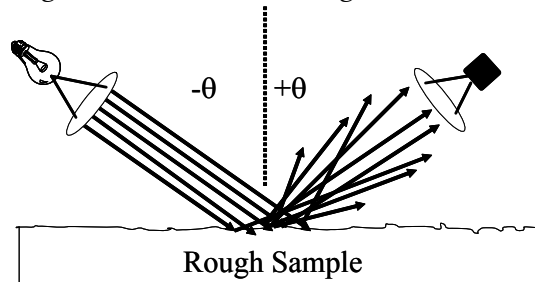
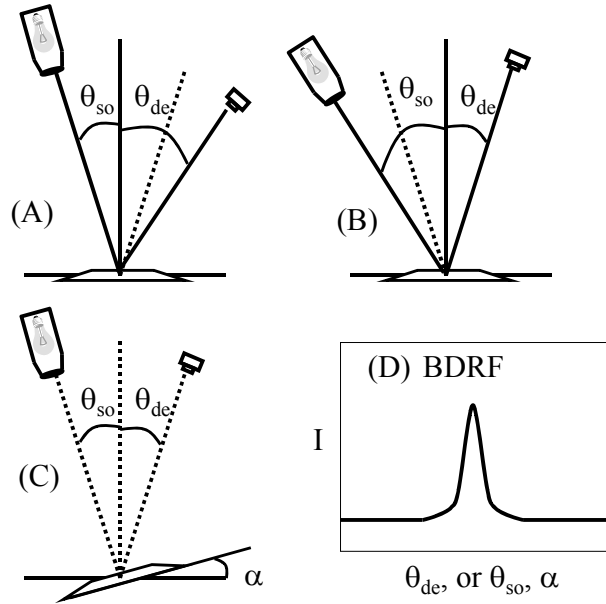


Figure 3: Surface roughness increases the angular distribution of specular light³



The angular distribution of reflected light can be measured with a goniophotometer (*gonio-* being Greek for angle), which measures reflected light as a function of angle of detection, θ_{de} , angle of source illumination, θ_{so} , or angle of tilt of the sample, θ , to produce the so-called bi-directional reflectance distribution function, BRDF². This is illustrated in Figure 4. The BRDF is a function of irradiance with respect to angle, meaning that the angular variations caused by roughness of surface material can be characterized by this curve. In this report, angles are expressed relative to the location of the peak, so $\alpha=0^\circ$ is the peak of the BRDF.

Figure 4: A goniophotometer measures reflect light as a function of (A) angle of detection θ_{de} , (B) angle of illumination θ_{so} and/or (C) surface tilt angle α , resulting in a (D) BRDF curve.



Surface topography is known to influence the results of gloss meter measurements^{4,6}. As per Figure 3, roughness in the surface disperses light over a range of angles, σ , where σ is defined as the RMS deviation about the mean specular angle, θ . A greater RMS deviation increases the width of the BRDF. Note that the specular angle θ is a property of the gloss meter, and σ is a property of the surface material⁴.

The collimating lens of a standard, non-goniophotometric gloss meter limits the gloss meter measurement to the specular angle $\theta \pm \theta_a$, where θ_a is the angular aperture of the detector³. When considering the surface topography model, the angular aperture, θ_a , is a crucially important factor to getting an accurate measurement, as it directly governs how much specular light gets accepted and how much gets rejected from the detector.

To make matters more difficult, it has been shown through research that the angular aperture θ_a is not identical for every manufacturer's gloss meter³. Differences of only 1-2° make a significant impact on the specular light measurement. Thus, standard gloss measurements are not easily relatable to the underlying mechanism of specular reflection from rough surfaces and are only significant relative to other measurements made with the same device. Thus, the current project employed a newly developed micro-goniophotometer to explore specular reflections from printing substrates.

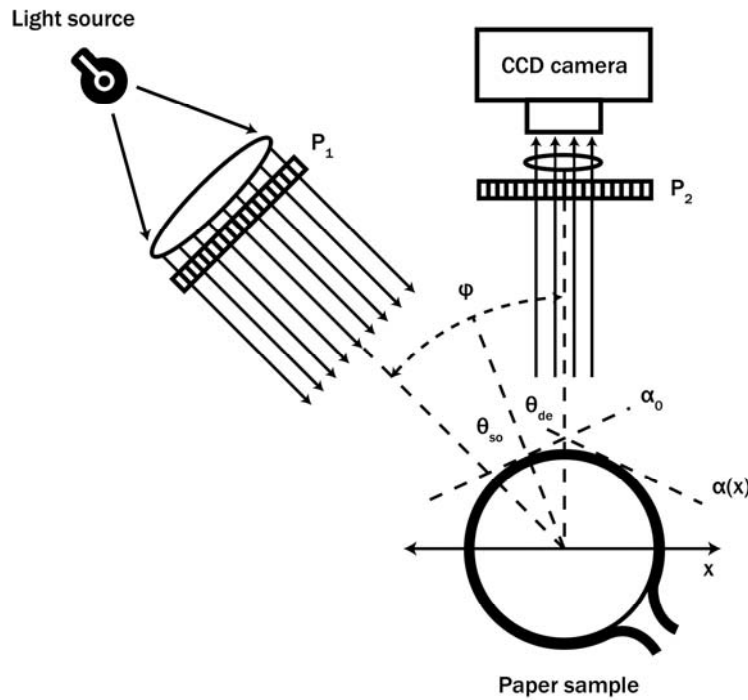
3 Experimental Methods

3.1 Instrument Design

The micro-goniophotometer used in this project combines the spatial scanning ability of a microdensitometer with a goniophotometer's ability to measure angular distribution¹. The hypothesis behind the design of this instrument is that both spatial resolution and angular resolution are required of a system in order to characterize the mechanism of specular reflection from complex surfaces.

Figure 5 is a schematic illustration of the micro-goniophotometer. A sample of printable substrate is wrapped around a cylinder and illuminated with collimated, linearly polarized light. A CCD camera is used to capture an image of the sample, and the camera is placed sufficiently far away to minimize parallax. Polarizers are used in front of the camera and the light source to separate Lambertian light from specular light, as described below.

Figure 5: *Geometry of the micro-goniophotometer. The y direction is collinear with the axis of the cylinder, and the x direction is through the cylinder. P_1 and P_2 are linear polarizing filters. This figure is not drawn to scale.*



The angle of illumination, θ_{so} , and the angle of detection, θ_{de} , are fixed. The tilt angle of the sample surface, α , is calculated from the horizontal location in the image, x , by using equation (1), where r is the radius of the cylinder.¹

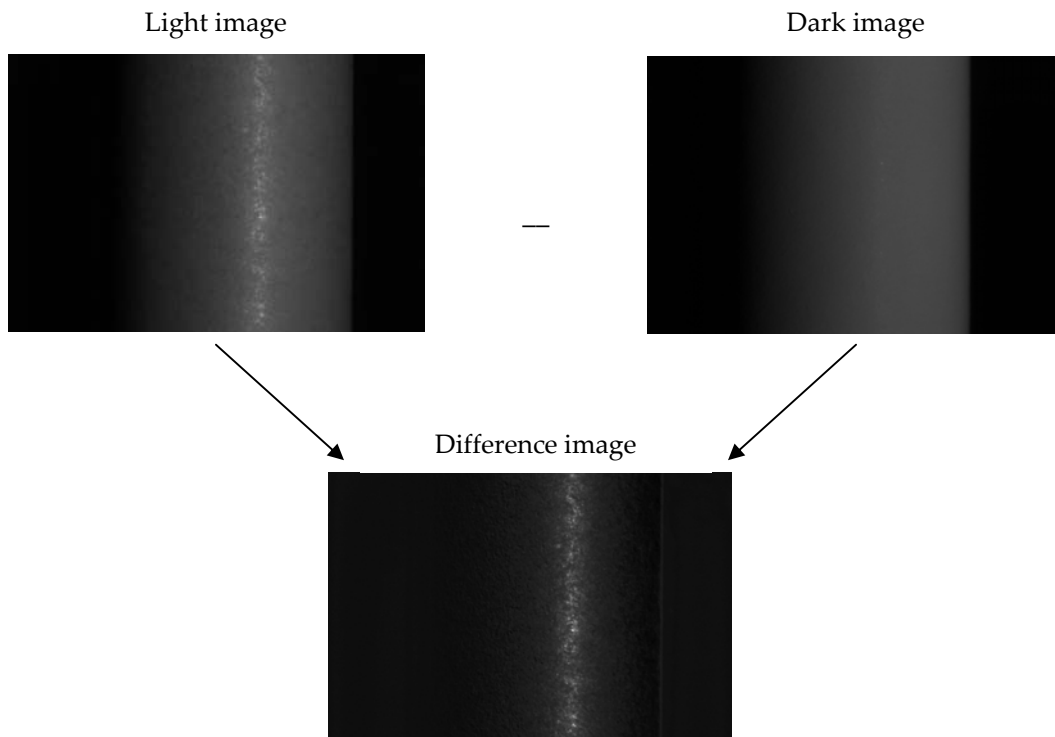
$$\alpha(x) = \sin^{-1}\left(\frac{x}{r}\right) \tag{1}$$

3.2 Data Collection

When attempting to quantify gloss characteristics, it is necessary to separate the specular reflection from the diffuse reflection. In order to generate meaningful data from the microgoniophotometer, a specific data collection method must be followed. To achieve this, two images of each sample are captured. The first is captured with the light source polarizer (P_1) and camera polarizer (P_2) aligned in parallel, in order to capture the full distribution of reflected light from the sample. This is nominally referred to as the “light” image. The other image needed for analysis is called the “dark” image and is captured with the polarizers aligned orthogonally. This alignment blocks the specular light, but allows the diffuse light through.

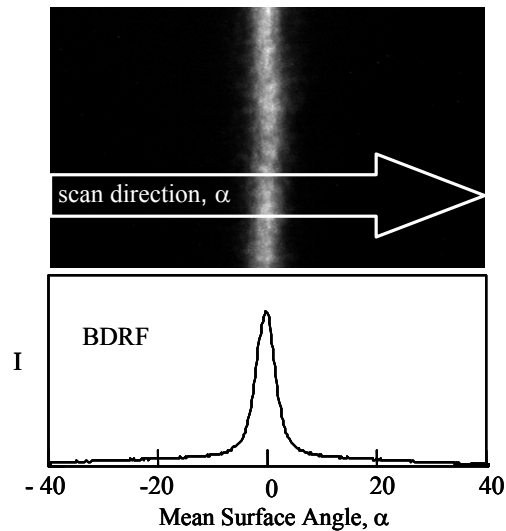
The final step in image generation is simply subtracting the dark image from the light image in software, which removes the diffuse reflection from the scene, leaving an image comprised only of specular reflectance. Figure 6 illustrates this process.

Figure 6: Sample images generated by the microgoniophotometer. A dark image ($P_1 - P_2 = 0^\circ$) is subtracted from a light image ($P_1 - P_2 = 90^\circ$) in software.



As mentioned before, the ultimate function of the system is generating a BRDF for each sample. This is achieved by simply scanning in the x direction of the difference image while averaging in the y direction. An example of this is shown in Figure 7.

Figure 7: Illustration of a difference image and its respective BRDF, generated by the micro-goniophotometer depicted in Figure 5.²



In this example image, the specular band is clearly visible, and its angular distribution is calculated from the known geometry of the cylinder using equation (1). A horizontal scan of the image yields its respective BRDF. The specular lobe is centered at $\alpha=0$, where the specular reflection from the sample is at a maximum. This is visible as the peak in the BRDF.

When a BRDF is measured by scanning across the source or detector angles, as is done with a traditional goniophotometer, each point on the BRDF corresponds to a different Fresnel specular angle, θ . By measuring reflectance versus sample angle, α , however, the resulting BRDF represents the angular distribution of light at a single, fixed specular angle, θ . As a result, the shape of the specular lobe in Figure 7 is a function of only of the topography of the sample, and the area under the lobe is proportional to the total Fresnel reflectance^{1,2}.

The advantage to this micro-goniophotometric system is that it allows a simultaneous measure of reflectance at different sample angles, α , rather than different angles of the source or detector, θ , as is more commonly done. Roughness in the surface topography spreads out the specular lobe over some width in the α direction^{1,4}. This is very useful to characterizing gloss because it incorporates an additional metric, σ , the RMS deviation of the surface angle, α , about the mean surface angle, $\alpha=0$.

It is often not computationally convenient to use the entire BRDF function for analysis operations, so a method of extracting a vector of BRDF features from the function is useful. A custom MathCAD worksheet was used to extract a vector of features from the BRDF. The feature vector included the peak height, width at several heights, granularity statistics, and standard gloss values taken at common measurement angles. In addition, each vector is preceded by an ID number and a single digit type index to identify its traditional classification by the paper manufacturers (see section II).

The MathCAD worksheet generates a 23 item vector of descriptive features, but the process is modular and open to additional measurement metrics if desired. Figure 8 shows a chart of the full description vector that was used. For the purposes of this project, analyses were only performed on certain features: BRDF area (A), peak height (h), half width ($w_{0.5}$), and RMS width (σ). In addition, a standard Gardner gloss meter was used to measure traditional gloss values at $\theta=20^\circ$, 60° and 85° .

Figure 8: Example description vector (sample #5).

Identification	Sample ID #	5
	Type Index	1
BRDF Area Statistics	A_{cum}	767.1686
	A	768.4335
	A_a	290.1074
	A_b	478.1364
	F_h	0.9276
RMS Width	F_a	0.3776
	σ_1	0.9419
Predicted Gloss	σ_2	19.89
	Ihara Gloss	40.33
BRDF Shape Statistics	BYK Gloss	45.28
	w_{0.5}	1.988
	w_{0.3}	2.556
	w_{0.1}	4.829
Granularity Statistics	h	132.4678
	Gran	0.7552
	GranMax	0.8903
	Qcorr	0.9747
Standard Gloss Values	R²	0.9958
	Std. Gloss 20°	48.3
	Std. Gloss 60°	76.6
	Std. Gloss 85°	98.9

4 Procedure

The experimental procedure involved using the microgoniophotometer to measure the BRDF curves of 50 unique samples of printable paper, which were generously provided by the Hewlett-Packard Corporation. The sample population included a diverse selection of samples including uncoated papers and papers with coatings of various transparency and opacity, in order to expose the system to a broad cross-section of typical printable papers.

Due to the large number of substrate samples, high repeatability was demanded from this project. The intensity of light from the fiber optic source was held constant throughout the data collection phase, as was the f-stop setting ($F/\# = 8$) on the camera lens. In addition, the entire apparatus was bolted down to an optical bench to insure that none of the necessary parts moved during data collection.

As a general rule implemented throughout the experiment, exposure settings were fixed such that no captured images yielded a pixel value of 255. This was done in order to ensure no loss of specular data due to exceeding the dynamic range of the image capture system. For certain high gloss samples, a neutral density filter ($ND = 0.5$) was placed in front of the lens in order to prevent saturation of light images.

Repeatability samples were taken during the weeks leading up to the main data acquisition phase. A series of 10 BRDFs were generated for a control sample, at a rate of 3-4 per week. Standard errors of metrics important to this project ($A, h, w_{0.5}, \sigma$) are displayed in Table 1.

Table 1: *Standard errors of BRDF metrics – 10 repeatability samples*

σ_A	18.03
σ_h	0.631
$\sigma_{w_{0.5}}$	0.319
σ_σ	0.146

Due to similarities in BRDF shape metrics and a distinct lack of image motion in the difference images, it was determined that the microgoniophotometric process was highly repeatable and sufficiently ready for the data acquisition phase.

Analysis of the BRDF data took the form of three main foci: analysis of BRDF area (A), analysis of BRDF shape characteristics ($h, w_{0.5}, \sigma$), and an attempt to correlate BRDF measurements with those from a standard gloss meter. Discussion of the findings from each analysis phase will be presented in sequential order.

4.1a BRDF Area Analysis

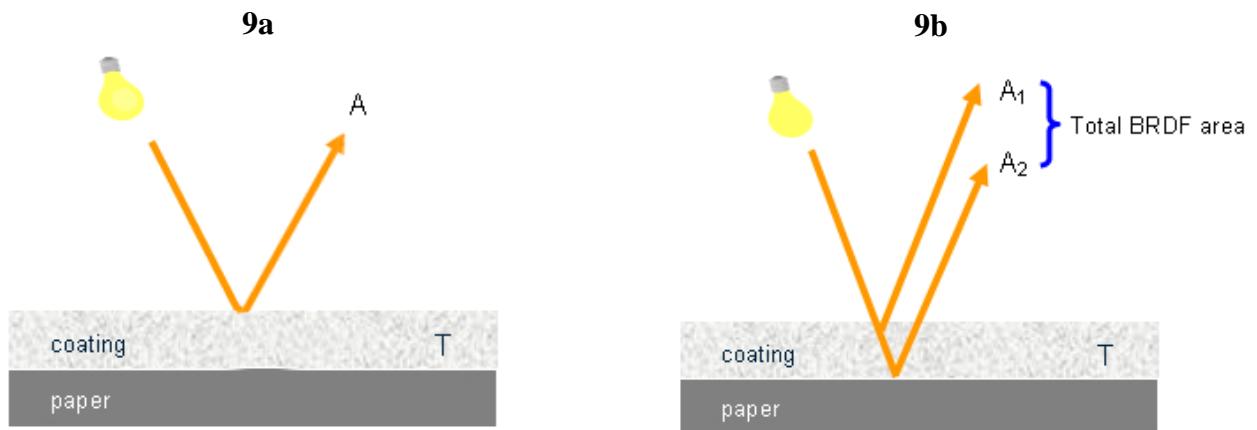
The area under the BRDF curve is a metric of unique significance. Unlike other BRDF shape characteristics that describe the distribution of the reflected light, BRDF area represents the total *quantity* of reflected light. Essentially, this is what one hopes to measure when utilizing a standard gloss meter, but research has led to the conclusion that this is not true (see Section III).

Since the BRDF represents specular irradiance as a function of incident angle, α , calculating the BRDF area requires a relatively simple integration, shown in Equation 2.

$$A = \int I(\alpha) d\alpha \quad (2)$$

Previous work has shown that specular light reflected from printed surfaces can include a significant amount of light reflected from surfaces below the first ink surface². This sub-surface reflection has been shown to increase the amount of specular light reflected from a printed sample by a factor of two for light that is not absorbed by the ink. A cyan ink, for example, was observed to reflect twice as much specular blue light than specular red light². This sub-surface effect is illustrated schematically in Figure 9.

Figure 9: Two models of specular reflection. Fig. 9a shows a single specular reflection; Fig. 9b illustrates the same sample with sub-surface reflections.



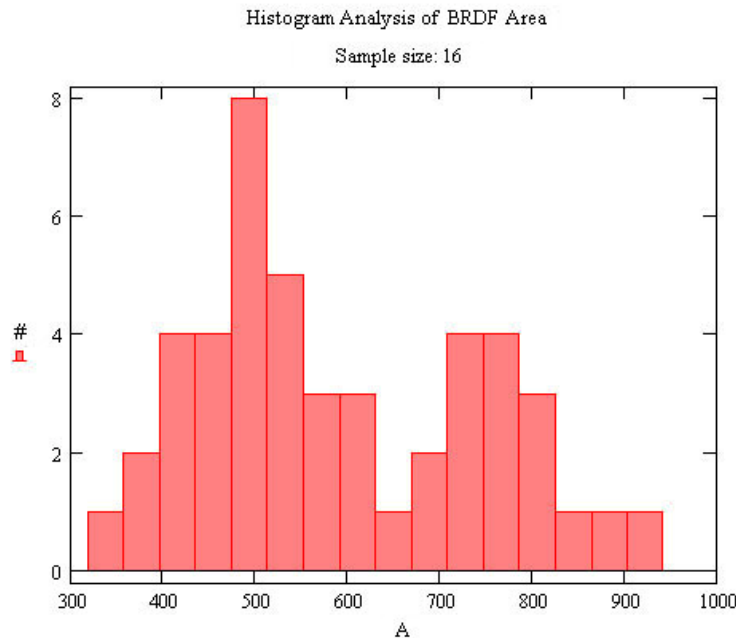
Since many printing papers are coated, and some of those coating are clear, it was anticipated that some printing papers would be found to have BRDF areas, A , that are twice the value of other papers. To explore this effect, a histogram analysis of BRDF area was conducted. BRDF area values for each sample were extracted from the

library of description vectors using MathCAD software. These values were then arranged in a simple histogram distribution, according to frequency of occurrence.

4.1b Results and Discussion

The histogram of BRDF area values is shown in Figure 10. The distribution of areas appears to be bimodal. Moreover, the papers in the right hand part of the area histogram are all coated papers. Non-coated papers, which are not able to show the sub-surface effect of Figure 9, are in the low area part of the area histogram. Many coated papers also fell in the low area part of the histogram. Most of the cast coated papers, which are known to have clear coatings, had areas in the right hand distribution. All of this is consistent with the hypothesis that a coating capable of not absorbing or significantly scattering light can produce a significant sub-surface contribution to the total specular light reflected from a paper. This indicates that high gloss can be achieved not only through forming a very smooth surface, but also by taking advantage of a sub-surface effect from a clear overcoat.

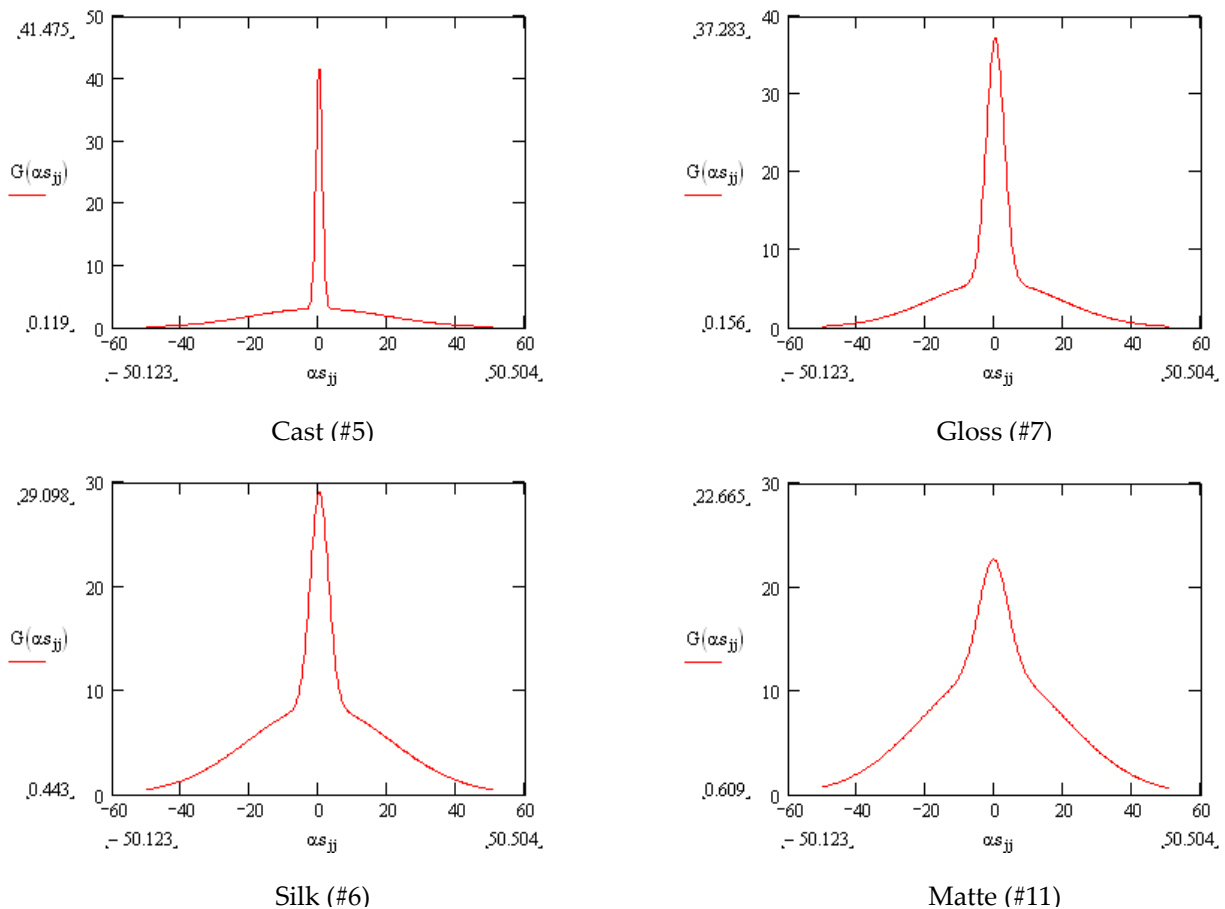
Figure 10: Histogram of frequency of BRDF area among sample population. The distribution appears to be bimodal, as expected.



4.2a BRDF Shape Analysis

For the purposes of this project, each paper sample was categorized upon delivery by Hewlett-Packard as one of four types: cast, silk, gloss, and matte. Cast papers are coated papers with an extremely smooth and flat finish that yields a high amount of specular reflectance distributed very closely about the mean angle. Gloss and silk papers are coated papers with less gloss. Figure 11 shows an example BRDF of each paper type. These graphics illustrate an important benefit of a full BRDF curve over a single gloss value: the BRDF curve provides much more information about the specular reflection process. The sharp spike of irradiance in the cast sample and broad distribution of light in the matte sample are particularly noticeable.

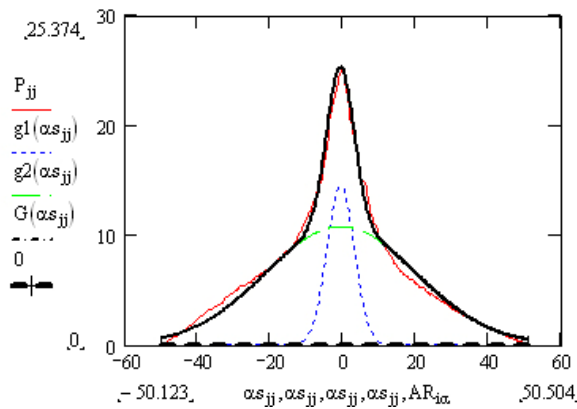
Figure 11: Example BRDFs of each paper classification.



Upon viewing the BRDF curve shapes, particularly for high gloss samples, it becomes apparent that there are two separate components of the curve shape: a clearly defined sharper component distributed about the mean, and a much broader component falling off to the sides. This behavior is not surprising for the cast coated

samples that show a total BRDF area of two, as discussed above. Presumably, the sub-surface reflection from the cast coated papers involves a broad component similar to the matte paper. It was found that the sum of two normal distributions provided a very good fit to the cast coated BRDFs. However, it was also found that most of the other BRDFs were also well fit by the sum of two normal distributions, and not fit well by a single normal distribution. Figure 12 illustrates this for a typical matte BRDF.

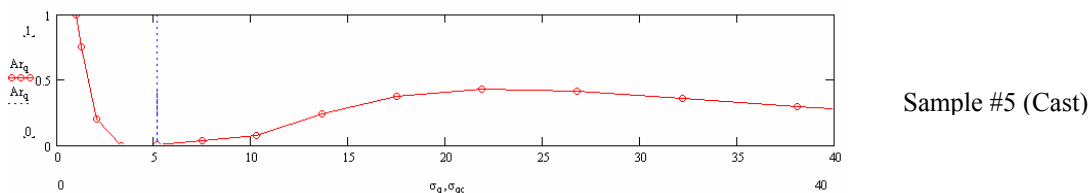
Figure 12: BRDF modeled as the sum of two Gaussian functions. The green and blue functions are the individual specular components, and the black line represents the total BRDF.

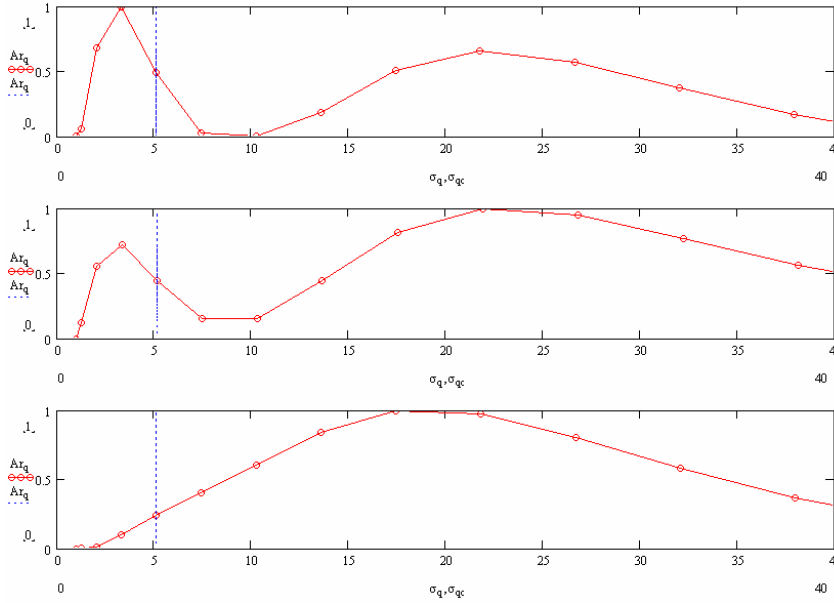


To further explore the shape characteristics of the BRDFs, a BRDF model function was constructed as the sum of 15 normal distributions, as shown in equation (3). Each of the Gaussian components was assigned a fixed width factor, σ , and the σ values were distributed between 1 and 38 degrees. The 15 height parameters, h , were adjusted to minimize the RMS deviation between the experimental BRDF and the model. The result was a vector of h values versus the width values, σ . Examples are shown in Figure 13.

$$\text{BRDF}(\alpha) = \sum_{i=1}^{15} h_i \cdot e^{\left\{ \frac{-\alpha^2}{2\sigma_i^2} \right\}} \quad (3)$$

Figure 13: Results of BRDF shape analysis - example shape spectra of samples from each classification.





Sample #19 (Gloss)

Sample #8 (Silk)

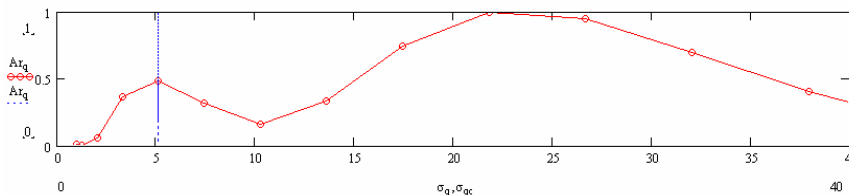
Sample #40 (Matte)

4.2b Results and Discussion

The technique of multi-gauss analysis was quite successful in showing the shape distribution of the BRDFs, as shown in Figure 13. The results of this analysis provide quantitative evidence to support the qualitative discussion of the shapes shown in Figure 11. As expected, the samples that were observed to have 2x areas in the area histogram analysis were observed to have two very pronounced shape components; one very sharp and narrow, and the other very broad. The cast coated sample in Figure 13 is an example. Also, some of the matte (non-coated) samples showed only the single, broad shape characteristic. This is consistent with the 1x area and the absence of a sub-specular reflection.

The surprising observation was that most samples, both coated and non-coated, displayed a two-width type of behavior, even though they displayed only a 1x area in the area histogram analysis. Figure 14 is an illustration for a matte sample. Clearly the matte sample can not display the same kind of sub-surface behavior that can occur in a cast coated sample with a transparent coating. This raises a questions about he origin of the bi-modal shape distribution of such samples. It appears that two specular reflection modes can occur even when sub-surface effects are not present.

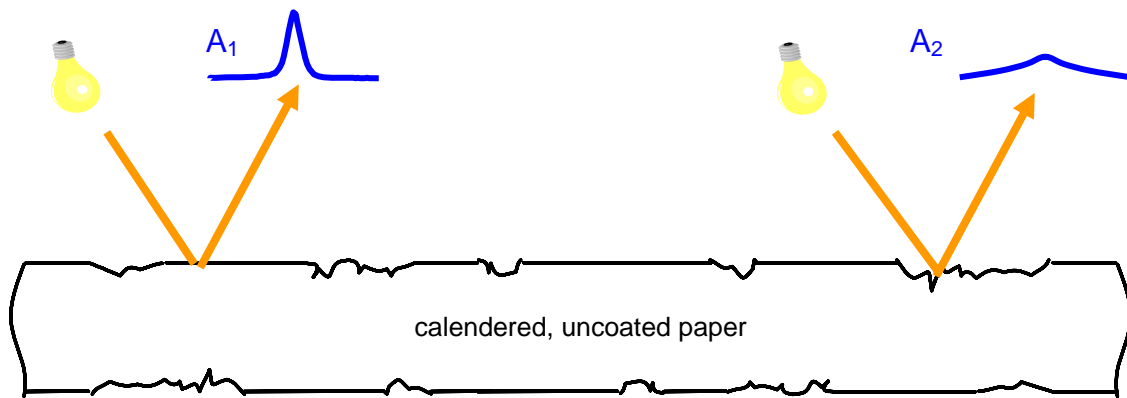
Figure 14: Shape spectra of sample #12 (matte).



Sample #12 (Matte)

A potential explanation for the bi-modal shape distribution observed for samples that do not show sub-surface specular reflections may be that the sample surface is composed of two distinct regions of roughness. This is illustrated schematically in Figure 15. According to this model, the surface is composed of rough regions randomly interspersed with more flattened regions. This semi-micro distribution of regions would produce an overall BRDF composed of the sum of two distribution curves. This model seems reasonable especially for matte samples which are typically calendered in manufacture. The calendering process presumably can flatten higher topographic regions of a sheet but leave lower regions with a rougher surface distribution. Further research would be useful to explore the effect of calendering on gloss.

Figure 15: Possible effects of calendering process on BRDF distribution.

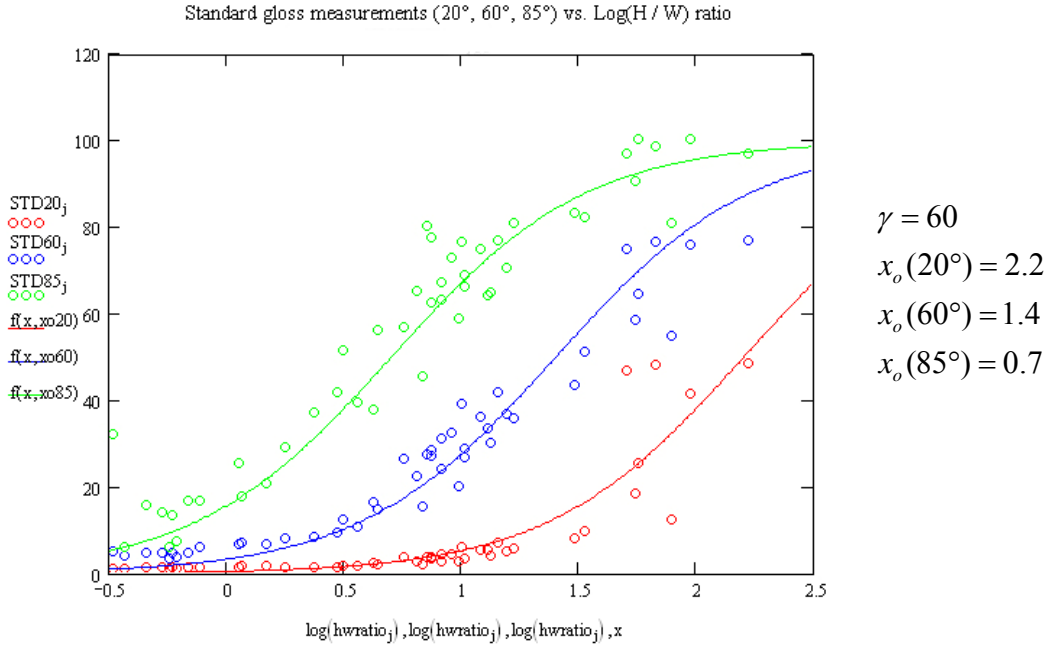


4.3a BRDF and Standard Gloss

A final study of the gloss process was explored by comparing the BRDF measurements with standard gloss measurements from a gloss meter. A BYK Gardner gloss meter was used to measure standard gloss at 20°, 60°, and 85° gloss angles, and correlates with data in the BRDF feature vector were sought. The result was the observation that standard gloss does not correlate well at all with the area, A , of the BRDF. Rather, a good correlation was observed between standard gloss and the log of the height/width ratio, defined as shown in equation (4). This is shown in Figure 16.

$$x = \log\left(\frac{h}{w_{0.5}}\right) \quad (4)$$

Figure 16: Standard gloss measurements approximated as a sigmoidal function of $\log(h/w_{0.5h})$



4.3b Results and Discussion

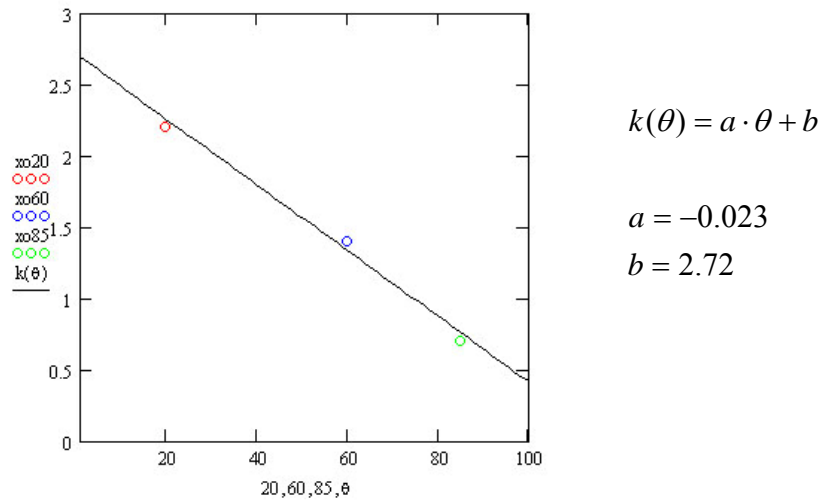
It was found that the data in Figure 16 were well modeled with a single function, shown in equation (5). This function has only two parameters, γ and x_o . The γ parameter governs the slope of the curve, and x_o governs the horizontal location of the curve.

$$Std. Gloss(x) = \frac{100}{1 + e^{\left[\frac{-4\gamma}{100}(x - x_o) \right]}} \quad (5)$$

The data is scattered, but a single slope parameter, $\gamma=60$, seems to fit all three gloss angles (20°, 60°, and 85°) quite well. Figure 17 shows the shift parameter, x_o , as a function of the gloss angle, θ , and it appears the relationship is a simple linear one. The implication seems to be that the shift parameter is a function of the gloss instrument (gloss angle, θ), and not a function of the sample. This seems to show that gloss measurements at different angles provide essentially the same information about the sample. However, that information does not appear to be related significantly to the specular reflectance factor. Rather, standard gloss appears to be a measure of the BRDF shape (height/width ratio). This may indicate that with appropriate calibration procedures, gloss meters of different geometry might be able to produce the same, reproducible results.

The scatter in the data shown in Figure 16 is greater than can be explained based on the experimental error of either the BYK Gardner gloss meter or the micro-goniophotometer. This indicates that the gloss measurements depend on some additional optical factors in addition to the width/height ratio. What this might be is not known, but it is clear that the relationship between BRDF and standard gloss measurement should be explored further.

Figure 17: Linear relationship between shifting coefficient (x_0) and standard gloss measurement angle.



5 Final Discussion and Conclusions

While data collection and analysis was a largely successful process, some experimental issues were raised that deserve further exploration. In particular, it seems the size of the cylinder used in the instrument should be larger than the 1 cm diameter used in this study. The 1 cm cylinder is not adequately large for wrapping of thick or delicate samples. Figure 18 shows an image of a sample that was very thick, almost like a card stock. This sample (#55) could not be wrapped around the mandrel without being creased, so it had to be removed from the sample population. In addition, the 1 cm cylinder was found to crack the coating on some coated sheets. An example is shown in Figure 19 for cast coated sample #5. These problems can easily be overcome with a larger diameter cylinder, but this would require re-configuration of the camera and lens optics if the same spatial resolution were to be maintained.

Figure 18: *Sample #55 (Neusiedler Color Copy, 200 gsm), creased when wrapped around the cylindrical mandrel.*

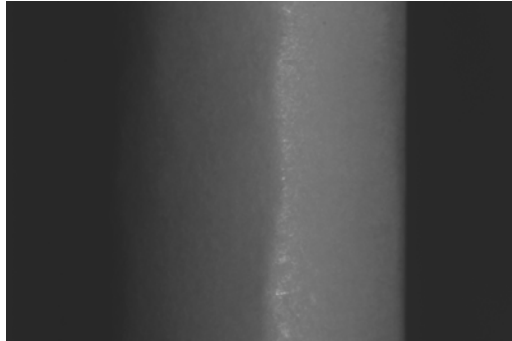
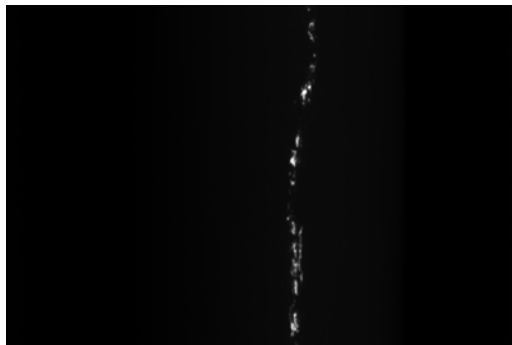


Figure 19: *Sample #5 (Xerox Digital Color Supergloss, 160 gsm), with a particularly delicate gloss coating that cracked when wrapped around the mandrel.*



Results from this research project clearly suggest that microgoniophotometric analysis is a promising method of specular gloss measurement that provides much more information about a sample than is available with conventional gloss meters or goniophotometers that rely on variations in source or detector angles to produce a BRDF. From the analysis of the BRDF data generated by this process, a series of conclusions can be drawn.

First, the area analysis suggests the presence of sub-surface specular reflections in a few of the coated sheets. However, this sub-surface effect appears not to contribute to gloss in most coated sheets. Presumably this is because most coatings scatter the light are too opaque to provide this effect.

The second conclusion is that the shapes of nearly all BDRF curves of printing substrates are well described by the sum of two normal distributions. Evidence further suggests two causes of this bi-component behavior. The first is the presence of sub-

surface reflections, and the second is the presence of surface regions of different surface roughness distributions.

The third significant conclusion is that a standard gloss meter does not measure a reflectance factor of the sample, but rather a factor of the sample's BRDF shape. Moreover, the results suggest the possibility of developing a calibration protocol that will unify gloss meter measurements regardless of the gloss angle, θ , one chooses to use.

The success of this project indicates that it would be worthwhile to continue the exploration of BRDF behavior of printing substrates. An examination of the spatial characteristics of specular gloss would be of particular interest. The instrument used in this project was designed to explore these spatial characteristics, but there was not sufficient time to do this in the current project.

6 References

1. J.S. Arney and Hoon Heo, "A Micro-Goniophotometer and Measurement of Print Gloss", *J.Imag.Sci. & Technol.*, in press 48:(2003).
2. J.S. Arney, P.G. Anderson, Geoffrey Franz, and William Pfiester, "Color Properties of Specular Reflections", *J.Imag.Sci. & Technol.*, in press 50:(2004).
3. J.S. Arney and P.G. Anderson, "The Geometry of 75° Gloss Measurements", *J.Imag.Sci. & Technol.*, in press 50:(2004).
4. Marie-Claude Béland, "Gloss Variation of Printed Paper: Relationship between topography and light scattering, Doctoral Thesis, KTH, Royal Institute of Technology, Stockholm, Sweden (1999).
5. M.-C. Béland and L. Mattson, "Optical Print Quality of Coated Papers", *J. Pulp Paper Sci.*, 23:10, J493 (1997).
6. Per-Åke Johansson, "Optical Homogeneity of Prints", Doctoral Thesis, KTH, Royal Institute of Technology, Stockholm, Sweden (1999).

7 Appendix

7.1 Index of Substrate Samples

Index #	Type	Name
5	Cast	Xerox Digital Color Supergloss
6	Silk	Xerox Digital Color Silk
7	Gloss	HP High Gloss
8	Silk	HP Soft Gloss 32#
9	Silk	HP Soft Gloss 28#
10	Silk	Boise Soft Gloss Color Laser
11	Matte	Domtar Microprint Coated Laser Matte
12	Matte	Domtar Luna Matte DI
13	Matte	MeadWestvaco Sterling Ultra 80 Matte Text
14	Cast	MeadWestvaco Sterling Ultra 8PT Cast Coated C1S
15	Gloss	Wausau Exact Gloss Coated
16	Gloss	Wausau Exact Gloss Coated
17	Gloss	MeadWestvaco Sterling Ultra Gloss Text
18	Silk	StoraEnso Futura Laser Dull Cover
19	Gloss	StoraEnso Futura Laser Gloss Cover
20	Gloss	Avery Color Laser Brochures Glossy Photo Quality
21	Gloss	m-real Silver Image Gloss
22	Gloss	sappi Voltage Gloss
23	Gloss	StoraEnso Futura Laser Gloss
24	Gloss	Xerox Digital Color Gloss
25	Gloss	Xerox Digital Color Gloss Cover
26	Gloss	HammerMill Color Copy Gloss
27	Cast	Rey Success Colorlaser SuperGloss
28	Cast	Xerox Digital Color Colotech Supergloss
29	Gloss	Rey Success Colorlaser Gloss
30	Silk	Xerox Colotech+ Silk Coated
31	Gloss	Xerox Colotech+ Gloss Coated
32	Cast	Canon Coated One Side Gloss Card Stock
33	Gloss	Canon Brochure Paper
34	Gloss	m-real Silver Image Gloss
35	Cast	Smart Paper Kromekote Laser High Gloss 1S Text
36	Matte	Xerox Phaser Trifold Brochures
37	Matte	Boise Cascade Presentation Laser
38	Matte	HP Premium Choice LaserJet Paper
39	Gloss	Great White Gloss Photo Paper 10% recycled
40	Matte	Great White Imaging & Photo Paper Matte Finish
41	Gloss	Oji Paper POD Gloss Coat
42	Gloss	Oji Paper POD Gloss Coat
43	Gloss	Oji Paper POD Gloss Coat
44	Matte	HP Color Paper Laser
45	Silk	StoraEnso Futura Laser Dull
46	Silk	StoraEnso Futura Laser Dull

47	Matte	HP Premium Choice LaserJet Paper
48	Matte	HP Premium Choice LaserJet Paper
49	Cast	Smart Papers Kromkote Laser High Gloss 2S Cover
50	Cast	Smart Papers Kromkote Laser High Gloss 2S Text
51	Matte	Boise Cascade Presentation Laser
52	Gloss	Xerox 1936 Glossy Paper
53	Matte	Neusiedler Color Copy
54	Matte	Neusiedler Color Copy
55	Matte	Neusiedler Color Copy